

Structure and Dynamics of CO₂ at the Air-Water Interface from Classical and Neural Network Potentials

Nitesh Kumar* , and Vyacheslav S. Bryantsev*

Chemical Sciences Division, Oak Ridge National Laboratory, Oak Ridge, Tennessee, 37831, United States

*E-mail: kumarn@ornl.gov, bryantsevv@ornl.gov

(Dated: February 7, 2025)

Abstract The accurate description of the structure and dynamics of CO₂ at the instantaneous air-water interface, along with the effects of surface fluctuations on the CO₂-transport processes, is essential for the development of negative emission technologies aimed to mitigate climate change. In this study, we performed molecular dynamics simulations of CO₂ at the air-water interface using neural network potentials (NNPs) trained on *ab initio* data generated through density functional theory-based molecular dynamics simulations. We compared these results with classical force fields to assess their performance in modeling interfacial CO₂ behavior. Our findings revealed that the asymmetric interactions, coupled with thermal surface fluctuations at the air-water interface significantly influence CO₂ transport into the aqueous phase. The simulations demonstrate that classical force fields underestimate both the free energy of CO₂ transport and the strength of its interactions at the interface compared to the neural network potentials. The free energy and the interfacial dynamics of CO₂ are primarily influenced by the distribution of water within the instantaneous interfacial water layer, responsible for creating asymmetric intermolecular interaction environment within the interfacial region.

Keywords: CO₂ Capture, Instantaneous Interface, Neural Network Potentials, Molecular Dynamics Simulations, Free Energy, Reaction Rates.

Aqueous solutions containing amine-based molecules is a promising class of absorbents for direct air capture (DAC) of CO₂. For CO₂ to traverse the gas/liquid boundary, it must pass through the interface. Although interfaces represent only a minor fraction of the total solvent molecules, they serve as crucial bottlenecks for controlling CO₂ transport and reactivity. A detailed molecular picture of how CO₂ moves from air into the aqueous phase and interacts with water and absorbents in the interfacial region could reveal valuable strategies to accelerate DAC.[1–3] A complete understanding of the CO₂ capture mechanism requires investigating CO₂ behavior at both neat and tailored interfaces.[4–6] This study aims to explore CO₂ behavior at the pure air–water interface using machine learning interatomic potentials trained based on density functional theory (DFT) calculations and contrasts them with the results from classical simulations that lack the explicit account of polarization effects.

The air-water interface forms a unique heterogeneous environment distinctly different from the bulk phase.[7–9] Characterizing CO₂ behavior at these dynamically evolving interfaces requires understanding how interfacial water structure and dynamics influence CO₂ adsorption, desorption, diffusion, and reaction rates.[10–16] The nanoscale region between air and water governs the flux at which CO₂ transfers into the aqueous phase,[17] where it subsequently interacts with absorbent molecules. The flux is indirectly affected by the anisotropy of intermolecular interactions between water and CO₂ within the instantaneous water surface, dictating the structuring and dynamics of CO₂ at this boundary. Previous studies of CO₂ at the aqueous interface have largely relied on ensemble-averaged descriptions, such as interfacial tension, width, and molecular orientation from such tech-

niques as Vibrational Sum-Frequency Generation spectroscopy (VSFG), Second Harmonic Generation (SHG), or X-ray spectroscopy.[18, 19] However, the role of interfacial barriers and solvent effects on CO₂ transport into the aqueous phase remains poorly understood. Classical models can enable the study of long timescale behavior but often lack accuracy, while *ab initio* molecular dynamics (AIMD) can provide a more accurate description, but limited to short timescales due to high computational expense.[20–22] To address this gap, we developed neural network potentials to describe the bulk and interfacial water in the presence of CO₂ trained on data from AIMD simulations performed using the revPBE density functional with the DFT-D3 dispersion correction. This choice of the DFT method provides a good balance between the accuracy and computational cost, given its superior performance in capturing both bulk and interfacial properties[23, 24] among the family of generalized gradient approximation (GGA) methods.[25] Although more advanced *ab initio* methods could enhance the quality of the NNP potentials, the required timescales and system sizes to develop such potentials and accurately capture interfacial properties remain difficult to achieve, even with current computational capabilities.[10, 26, 27]

Using neural network potentials,[28, 29] we aimed to improve the accuracy of classical potentials to describe the structure and dynamics of CO₂ in the interfacial region. This work characterizes the interfacial chemical processes controlling the transport of CO₂ through the interfacial phase boundary. Understanding these processes is crucial to develop a complete understanding of the direct air capture of CO₂ at the air/water interface and explain why CO₂ reactions with amino acids are kinetically accelerated at these interfaces, as revealed by

our recent study.[30] Herein, we find that the free energy of CO₂ transport from the air to the aqueous phase is influenced by the distribution or the spread of instantaneous water molecules, creating a unique coordination environment for interfacial CO₂.[31, 32]

In this study, extensive AIMD simulations were carried out on 3 bulk and 4 air/water interface systems. Each system was simulated for at least 40 ps, with a total of over 280 ps of AIMD simulations. From these simulations, 280,000 snapshots were extracted and used to train the NNP models, with details provided in the SI. We then employed the trained neural network potentials in LAMMPS patched with DeepMD-kit to simulate air-water systems with two interfaces, initially placing CO₂ randomly in the simulation cell at a partial pressure of about 0.145 atm. This pressure, which is relevant for direct air capture, is sufficiently low to accurately compute interfacial properties while minimizing CO₂ clustering and bubble formation observed at higher concentrations.[34] We performed additional simulations doubling the CO₂ concentration and observed a similar potential of mean force (PMF) for CO₂ along the *z* axis (Figure S6). This indicates that at the studied concentrations, the PMFs remains almost unaffected, validating our system for investigating structure and dynamics under DAC conditions. However, further increases in CO₂ concentration would begin to impact interfacial properties such as interfacial tension and width. The analysis of the interfacial systems by Niblett et al. suggests that the results for certain properties such as water density distribution and orientation remain largely unaffected when explicitly modeled long-range effects are introduced.[28, 35] Recent studies showed that a comprehensive training on both bulk and interfacial systems can provide more accurate description of the interface, where the symmetry of the intermolecular interactions is broken and the long-range interactions are anisotropic. In this study, we followed this strategy of extensive training, ensuring that both the bulk and interfacial results are comparable. Importantly, in the systems without ions present at the interface, it is indeed possible to achieve accurate results without a significant increase in error for interfacial systems.[36] The RMSE in energy and forces are obtained to be < 1 meV/atom and < 100 meV/Å respectively for both bulk and interface (Table S1), showing similar errors for trained NNP model. In cases where ions are introduced, explicit treatment of long-range electrostatics may be required to capture the correct behavior. Additional technical details are provided in the SI.

Herein, we first compared the radial distribution functions (RDFs) and coordination numbers between O_{H₂O} atoms in the bulk aqueous phase, modeled using AIMD and two NNP models, with cutoff radii of 7 Å and 8 Å. Two cutoffs were tested to ensure they adequately captured the intermolecular interactions between CO₂ and water. The RDFs were compared against experimental RDF data from reference 33. Our pair-correlation results indicate only minimal deviations in the RDFs be-

tween the AIMD and NNP models, with the AIMD simulations exhibiting good agreement with the water-water interactions similar to previous AIMD studies (Figure 1 A and B).[37] Moreover, the NNP models demonstrated excellent consistency with AIMD in terms of water coordination numbers. Recognizing that CO₂ can interact with water at two distinct sites—either the carbon atom (C_{CO₂}) with the oxygen atom (O_{H₂O}) or the oxygen atom (O_{CO₂}) with the hydrogen atom (H_{H₂O})—we computed the RDF and coordination numbers for both interaction types (Figure 1 C-F). The overall shapes of the CO₂-H₂O interaction RDFs are consistent with previous studies.[38–41] The smaller cutoff (7 Å), slightly overestimated coordination numbers for CO₂-water interactions, whereas the larger cutoff of 8 Å accurately reproduced experimental structural arrangements. This highlights the importance of using larger cutoffs to accurately model structural properties of weakly bound CO₂.

We then characterized the distribution of CO₂ at the air-water interface in terms of the density profiles along the *z*-axis (Figure 2). We observe that the NNP force fields showed a greater density of CO₂ within the interfacial region compared to the SPC/E and two other classical water models (TIP4P and TIP5P) (Figure S7). The respective PMFs associated with CO₂ adsorption within the interfacial region show significant difference in the well depth and the barriers associated with both the desorption of CO₂ from the interface and the transport of CO₂ to the aqueous phase (Figure 2).

For both NNP and classical models, the desorption barrier of CO₂ from the interface to the air phase is observed to be lower than the barrier for transport into the aqueous phase. The free energy of CO₂ desorption from the classically modeled interface to the air phase is ~ -0.7 kcal/mol lower than that from the NNP-modeled interface (Figure 2). Similarly, the free energy required for CO₂ transport from the interface to the aqueous phase is ~ -0.65 kcal/mol lower for the classical model compared to the NNP model. Other classical models showed similar PMFs compared to SPC/E (Figure S7). Despite these variations, both the NNP and classical models reveal consistent differences in the thermodynamics of CO₂ adsorption and desorption. Collectively, these results suggest that a CO₂ molecule at the interface is more likely to move to the air phase than into the aqueous phase. To quantify how these barriers affect the rates of transport, we employed transition state theory in the harmonic approximation to obtain and compare the rate constants (*k*) for CO₂ desorption and transport into the aqueous phase using the equation:

$$k = \frac{k_B T}{h} e^{-\Delta W/k_B T},$$

where, *h* is the Planck constant, *T* is the temperature and *k_B* is the Boltzmann constant, ΔW represents the free energy barrier for CO₂ desorption to the air phase or transport into the aqueous phase. To obtain the relative

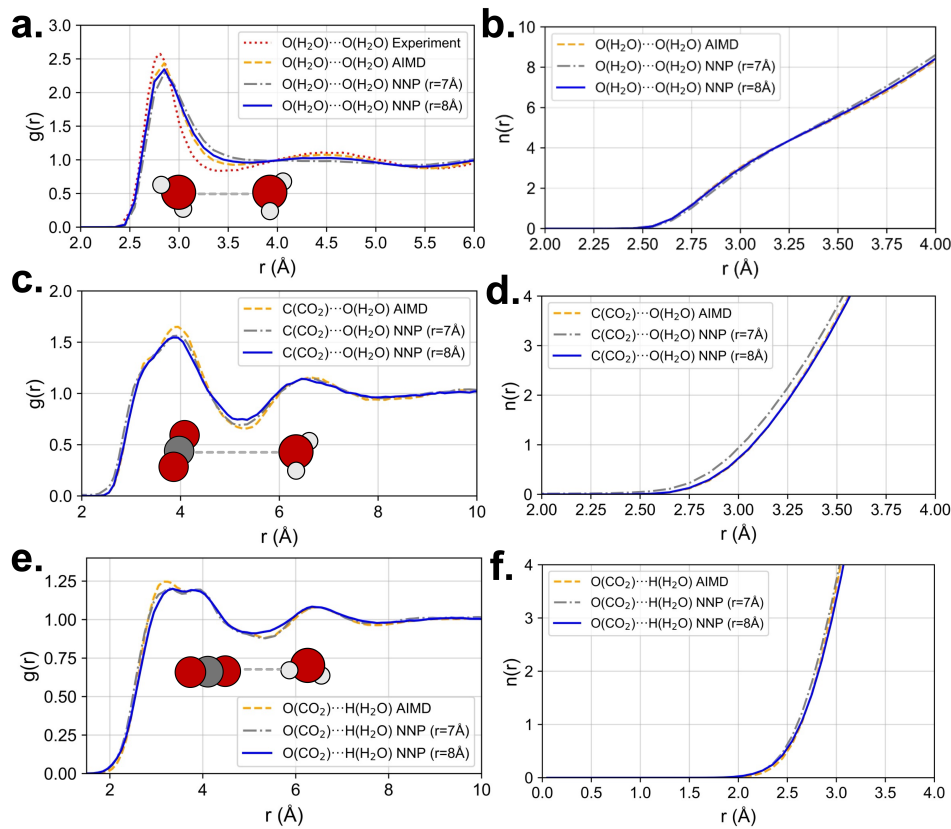


FIG. 1: The radial distribution function and coordination number between (a,b) O_{H₂O}-O_{H₂O} (c,d) C_{CO₂}-O_{H₂O} and (e,f) O_{CO₂}-H_{H₂O} obtained in the bulk aqueous phase modeled obtained from AIMD simulations, NNP simulations with two different cutoffs (7 and 8 Å) used in the NNP training. The experimental radial distribution between O_{H₂O} molecules used for comparison with AIMD and NNP radial distribution function is taken from ref. 33.

differences in the rates between the NNP and classical model, we used

$$\ln \frac{k_{\text{NNP}}}{k_{\text{classical}}} = - \frac{\Delta W_{\text{NNP}} - \Delta W_{\text{classical}}}{k_B T},$$

where k_{NNP} , ΔW_{NNP} , $k_{\text{classical}}$, and $\Delta W_{\text{classical}}$ represent the rate constants and free energy barriers for the NNP and classical models, respectively. For the classical model, the difference in barriers results in a desorption rate that is $\sim 2.3 \times$ faster for CO₂ desorption from the interface to the air phase than for CO₂ transport into the aqueous phase. In the case of the NNP model, CO₂ desorption is $\sim 3.0 \times$ faster than its transport to the aqueous phase. For both systems, the desorption rate of interfacial CO₂ is faster than its transfer into the aqueous phase because, unlike air, CO₂ must penetrate the interfacial hydrogen-bonding network, moving layer by layer—such as from interfacial water layers 1 to 5 (which have intrinsic viscosity) before reaching the bulk.[42–44] This process is energetically less favorable, leading to slower transport rates of CO₂ phase transfer into the aqueous phase. These results highlight that the asymmetric interactions at the air-water interface play a significant role in governing the free energies of CO₂ transport, ultimately

influencing the rates of CO₂ uptake into the aqueous phase.[39]

It is important to understand the role of fixed charge distribution at the interface in stabilizing CO₂ within the interfacial region. Therefore, we computed the electrostatic potential along the z -axis for both the classical and NNP models (Figure 3). The electrostatic potential, based on the interactions along the z -axis, is calculated using the equation:

$$\Phi(z) = \frac{1}{\epsilon_0 \epsilon_r} \int_0^z \int_0^{z'} \rho_c(z'') dz'' dz',$$

where ϵ_0 is the vacuum permittivity, ϵ_r is the relative permittivity (taken as 1), and $\rho_c(z)$ represents the charge density distribution along the z -axis.[45–47] Since the NNP model does not directly provide atomic charges, we applied classical atomic charges obtained from the SPC/E water model to the coordinates obtained from the NNP simulations. We found that CO₂ in the classical model would be electrostatically more strongly attracted to the interface, which exhibit a more negative electrostatic potential (~ -0.3 V) compared to the NNP model. If these interaction are key then CO₂ molecules,

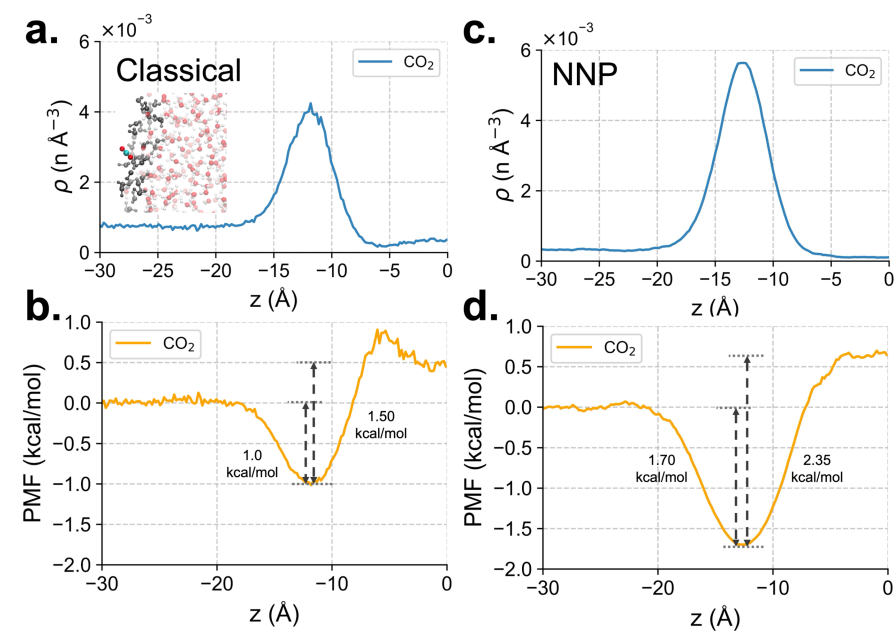


FIG. 2: (a.) Number density profiles and the (b.) potential of mean force of the distribution of CO_2 at the air-water interface modeled using the classical potentials (SPC/E for water and TRAPP-flex for CO_2). (c.) Number density profiles and the (d.) potential of mean force of the distribution of CO_2 at the air-water interface modeled using the neural network potentials. An illustration of the water and CO_2 in the instantaneous water layer (black) is provided in the inset of part (a.)

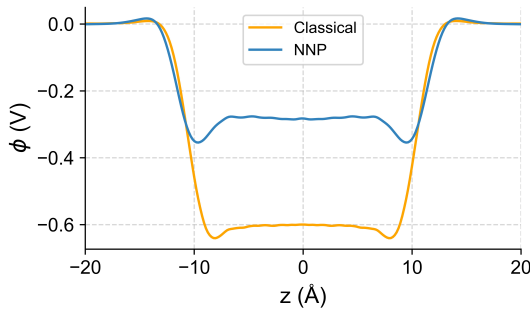


FIG. 3: Electrostatic potential along the z -axis for both the systems modeled using the classical and neural network potentials. We used the classical charges and NNP simulation coordinates to obtain the electrostatic potential profiles.

whether in the air or aqueous phase, would be more likely drawn to the interface in the classical model than in the NNP model. In contrast, the PMF analysis shows that CO_2 move more easily between the two phases in the classical model due to lower energy barriers, as compared to the NNP model. The opposite trends between the electrostatic potential profile and PMF data indicate that, while electrostatic potential based on fixed point charges reveals local electric fields and potential wells at the interface,[48, 49] it does not fully capture the free energy landscape governing molecular transport. The latter includes electrostatic contributions from induced charges and polarization together with the thermally induced sur-

face fluctuations, and solvent effects from asymmetric interactions with interfacial water molecules. To get more details into the solvent effects, we computed the radial distribution function (RDF) between the carbon atom of CO_2 (C_{CO_2}) and the oxygen atom of water ($\text{O}_{\text{H}_2\text{O}}$) at the interface using instantaneous interface definitions.[50, 51] Likewise PMFs on Figure 2, the RDFs (Figure S8) show stronger interactions between CO_2 and water in the NNP model compared to the classical model, pointing to differences in the solvent effects controlling CO_2 transport across the liquid phase boundary.

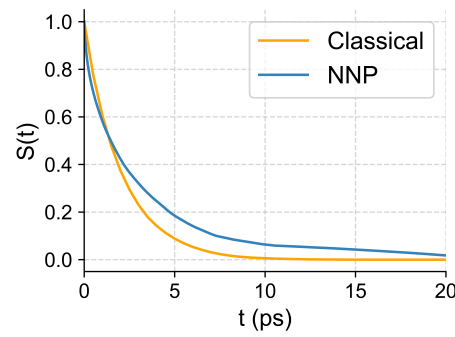


FIG. 4: The survival probabilities of CO_2 in the instantaneous water layer of the air-water interface for the systems modelled using classical and neural network potentials.

In the classical model, the weaker total solvation effects at the interface results in CO_2 moving back and forth

between the interface and either the air or bulk aqueous phase, decreasing its residence time in the truly interfacial layer and speeding up its dynamics at the interface. To investigate this behavior further, we computed the survival probability of CO₂ in the interfacial layer. Specifically, we calculated the probability of finding CO₂ at a later time t , given its presence in the instantaneous layer at $t = 0$ (Figure 4). The results showed that the survival probability decayed more rapidly in the classical model compared to the NNP model, indicating faster dynamics of CO₂ at the air-water interface when modeled with classical potentials. Similarly, faster dynamics of H₂O was observed in the classical system compared to the NNP system (Figure S9).

Moreover, we observed significant differences in the spread of the PMF and electrostatic potential (due to wider charge density distribution, Figure S10), which we attribute to variations in the surface fluctuations at the interfaces modeled using classical and NNP potentials. To quantify the extent of these surface fluctuations, we employed a method similar to that described in ref. 52. First, we computed the density profiles of water and CO₂ in the instantaneous layers (Figure S11). These density profiles were fitted to the Gaussian distribution function and the standard deviation σ is used to compute the Full Width at Half Maximum (FWHM) as $2\sqrt{2\ln(2)}\sigma$, which is used to characterize the spread of the surface fluctuations (Figure S11).[42] The FWHM was calculated to be 2.94 Å for the classical model and 3.07 Å for the NNP model, indicating that water is more widely spread at the interface in the NNP model. This wider spread of interface leads to larger surface fluctuations compared to the classical model, possibly contributing to the free energy associated with the CO₂ transport from air to the aqueous phase.[53] As a result, significant differences in the charge distribution (Figure S10) and orientation of water at the interface were observed between the two models (Figure 5).

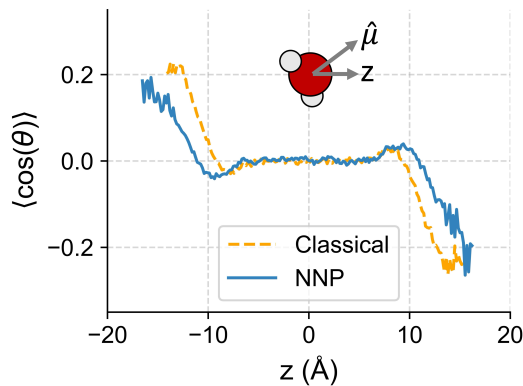


FIG. 5: Water dipole orientation along the z -axis for both air/CO₂/water systems modeled using the classical and neural network potentials.

Specifically, in the NNP model, water molecules demonstrate a more pronounced spread of water tilted

toward the air phase (with similar maximum cos values) within the interfacial region (the overall water orientation behavior is consistent with previously observed DFT-MD results[54]) compared to the classical model. This pronounced tilt—where the hydrogen atoms of H₂O are more oriented (thicker water layer showing tilt in the NNP model compared to classical water model) toward the air—along with slower water dynamics (as shown by the water O-H vector orientation in Figure S12), creates favorable configurations for stronger interactions between water and CO₂. Consequently, the free energy barrier for CO₂ transport from the interface into the aqueous phase rises, driven by the combined effects of enhanced surface fluctuation-induced capillary waves, extended molecular orientation, and improved solvation.[36, 55]

In summary, we studied the structure and dynamics of CO₂ at the air-water interface using machine learning simulations and compared the results with classical force-fields simulations. Our findings reveal significant differences in the distribution, dynamics, and free energy associated with CO₂ transport to the aqueous phase. Specifically, we observed that the classical force fields underestimated the free energy barrier for CO₂ transport and exhibited weaker interactions between CO₂ and H₂O at the air-water interface compared to neural network potentials. First-principles accuracy is essential for computing CO₂ thermodynamics and kinetics at evolving interfaces, as these simulations inherently include explicit polarization effects necessary for accurately describing interfacial chemical and transport processes. Despite stronger interfacial electrostatic potential from a fixed point-charge model, CO₂ interacts weaker with classical water. These weaker interactions resulted in faster adsorption and desorption kinetics at the air-water interface. We observed enhanced surface fluctuations and interface broadening for the NNP compared to the classical model. The contributions from the thermal surface fluctuations and solvent rearrangements are often overlooked but are essential for accurately characterizing chemical reactions and transport processes at the interface, and should be considered when using computational methods to model interfacial chemical reactions and transport properties.

Acknowledgments

This research was supported by the US Department of Energy, Office of Science, Basic Energy Sciences, Chemical Sciences, Geosciences, and Biosciences Division, Separation Sciences. This work was produced by UT-Battelle LLC under Contract No. AC05-00OR22725 with the U. S. Department of Energy. This research used resources of the Oak Ridge Leadership Computing Facility at the Oak Ridge National Laboratory, which is supported by the Office of Science of the U.S. Department of Energy under Contract No. DE-AC05-00OR22725.

Supplementary Information

Methodology, parity plots, density profiles, radial distribution functions, survival probabilities, and potentials of mean force.

Public Access Statement

This manuscript has been authored by UT-Battelle, LLC, under contract DE-AC05-00OR22725 with the US Department of Energy (DOE). The US government retains and the publisher, by accepting the article for publication, acknowledges that the US government retains a nonexclusive, paid-up, irrevocable, worldwide license to publish or reproduce the published form of this manuscript, or allow others to do so, for US government purposes. DOE will provide public access to these results of federally sponsored research in accordance with the DOE Public Access Plan (<http://energy.gov/downloads/doe-public-access-plan>).

References

- [1] Guo, D.; Thee, H.; Tan, C. Y.; Chen, J.; Fei, W.; Kentish, S.; Stevens, G. W.; da Silva, G. Amino acids as carbon capture solvents: chemical kinetics and mechanism of the glycine+ CO₂ reaction. *Energy & fuels* **2013**, *27*, 3898–3904.
- [2] Gladich, I.; Abotaleb, A.; Sinopoli, A. Tuning CO₂ capture at the gas/amine solution interface by changing the solvent polarity. *The Journal of Physical Chemistry B* **2020**, *124*, 10245–10256.
- [3] Martins-Costa, M. T.; Ruiz-López, M. F. Reactivity of Monoethanolamine at the Air–Water Interface and Implications for CO₂ Capture. *The Journal of Physical Chemistry B* **2024**, *128*, 1289–1297.
- [4] Kumar, N.; Premadasa, U. I.; Dong, D.; Roy, S.; Ma, Y.-Z.; Doughty, B.; Bryantsev, V. S. Adsorption, Orientation, and Speciation of Amino Acids at Air–Aqueous Interfaces for the Direct Air Capture of CO₂. *Langmuir* **2024**, *40*, 14311–14320.
- [5] Premadasa, U. I.; Kumar, N.; Zhu, Z.; Stamberg, D.; Li, T.; Roy, S.; Carrillo, J.-M. Y.; Einkauf, J. D.; Custelcean, R.; Ma, Y.-Z. et al. Synergistic Assembly of Charged Oligomers and Amino Acids at the Air–Water Interface: An Avenue toward Surface-Directed CO₂ Capture. *ACS Applied Materials & Interfaces* **2024**, *16*, 12052–12061.
- [6] Sinopoli, A.; Abotaleb, A.; Pietrucci, F.; Gladich, I. Stability of a monoethanolamine-CO₂ zwitterion at the vapor/liquid water interface: implications for low partial pressure carbon capture technologies. *The Journal of Physical Chemistry B* **2021**, *125*, 4890–4897.
- [7] Bjorneholm, O.; Hansen, M. H.; Hodgson, A.; Liu, L.-M.; Limmer, D. T.; Michaelides, A.; Pedevilla, P.; Rossmeisl, J.; Shen, H.; Tocci, G. et al. Water at interfaces. *Chemical reviews* **2016**, *116*, 7698–7726.
- [8] Zarayeneh, N.; Kumar, N.; Kalyanaraman, A.; Clark, A. E. Dynamic Community Detection Decoupling Multiple Time Scale Behavior of Complex Chemical Systems. *Journal of Chemical Theory and Computation* **2022**, *18*, 7043–7051.
- [9] Kumar, N.; Clark, A. E. Adsorbate Organization Characterized by Sublevelset Persistent Homology. *Journal of Chemical Theory and Computation* **2023**, *19*, 3303–3312.
- [10] Brookes, S. G.; Kapil, V.; Schran, C.; Michaelides, A. The wetting of H₂O by CO₂. *The Journal of Chemical Physics* **2024**, *161*.
- [11] Martins-Costa, M. T.; Ruiz-López, M. F. The Structure of Carbon Dioxide at the Air-Water Interface and its Chemical Implications. *Chemistry—A European Journal* **2024**, e202400825.
- [12] Tarbuck, T. L.; Richmond, G. L. Adsorption and Reaction of CO₂ and SO₂ at a Water Surface. *Journal of the American Chemical Society* **2006**, *128*, 3256–3267.
- [13] Shiga, M.; Morishita, T.; Sorai, M. Interfacial tension of carbon dioxide-water under conditions of CO₂ geological storage and enhanced geothermal systems: A molecular dynamics study on the effect of temperature. *Fuel* **2023**, *337*, 127219.
- [14] Kumar, N. *Chemical and Transport Phenomena at Biphase Interfaces*; Washington State University, 2023.
- [15] England, A. H.; Duffin, A. M.; Schwartz, C. P.; Uejio, J. S.; Prendergast, D.; Saykally, R. J. On the hydration and hydrolysis of carbon dioxide. *Chemical Physics Letters* **2011**, *514*, 187–195.
- [16] Kumar, N.; Bryantsev, V. S.; Roy, S. The Role of Nonequilibrium Solvent Effects in Enhancing Direct CO₂ Capture at the Air–Aqueous Amino Acid Interface. *Journal of the American Chemical Society* **2025**, *147*, 1411–1415, PMID: 39711150.
- [17] House, W. A.; Howard, J. R.; Skirrow, G. Kinetics of carbon dioxide transfer across the air/water interface. *Faraday Discussions of the Chemical Society* **1984**, *77*, 33–46.
- [18] Xu, M.; Spinney, R.; Allen, H. C. Water structure at the air–aqueous interface of divalent cation and nitrate solutions. *The Journal of Physical Chemistry B* **2009**, *113*, 4102–4110.
- [19] Liang, Z.; Bu, W.; Schweighofer, K. J.; Walwark Jr, D. J.; Harvey, J. S.; Hanlon, G. R.; Amoanu, D.; Erol, C.; Benjamin, I.; Schlossman, M. L. Nanoscale view of assisted ion transport across the liquid–liquid interface. *Proceedings of the National Academy of Sciences* **2019**, *116*, 18227–18232.
- [20] Behler, J. Neural network potential-energy surfaces in chemistry: a tool for large-scale simulations. *Physical Chemistry Chemical Physics* **2011**, *13*, 17930–17955.
- [21] Duignan, T. T. The Potential of Neural Network Potentials. *ACS Physical Chemistry Au* **2024**, *4*, 232–241.
- [22] Ma, X.; Bryantsev, V. S.; Roy, S. An ab initio free energy study of the reaction mechanism and rate-limiting steps of CO₂ capture by aqueous glycine. *Cell Reports Physical Science* **2023**, *4*.
- [23] Todorova, T.; Seitsonen, A. P.; Hutter, J.; Kuo, I.-F. W.; Mundy, C. J. Molecular dynamics simulation of liquid water: hybrid density functionals. *The Journal of Physical Chemistry B* **2006**, *110*, 3685–3691.
- [24] Forster-Tonigold, K.; Groß, A. Dispersion corrected RPBE studies of liquid water. *The Journal of chemical physics* **2014**, *141*.
- [25] Gillan, M. J.; Alfe, D.; Michaelides, A. Perspective: How good is DFT for water? *The Journal of chemical physics* **2016**, *144*.

- [26] Piaggi, P. M.; Weis, J.; Panagiotopoulos, A. Z.; Debenedetti, P. G.; Car, R. Homogeneous ice nucleation in an ab initio machine-learning model of water. *Proceedings of the National Academy of Sciences* **2022**, *119*, e2207294119.
- [27] McGrath, M.; Siepmann, J.; Kuo, I.-F.; Mundy, C. Vapor–liquid equilibria of water from first principles: comparison of density functionals and basis sets. *Molecular Physics* **2006**, *104*, 3619–3626.
- [28] Niblett, S. P.; Galib, M.; Limmer, D. T. Learning intermolecular forces at liquid–vapor interfaces. *The Journal of chemical physics* **2021**, *155*.
- [29] Montero de Hijes, P.; Dellago, C.; Jinnouchi, R.; Schmiedmayer, B.; Kresse, G. Comparing machine learning potentials for water: Kernel-based regression and Behler–Parrinello neural networks. *The Journal of Chemical Physics* **2024**, *160*.
- [30] Kumar, N.; Bryantsev, V. S.; Roy, S. The Role of Nonequilibrium Solvent Effects in Enhancing Direct CO₂ Capture at the Air–Aqueous Amino Acid Interface. *Journal of the American Chemical Society* **0**, *0*, null, PMID: 39711150.
- [31] Leitold, C.; Mundy, C. J.; Baer, M. D.; Schenter, G. K.; Peters, B. Solvent reaction coordinate for an SN₂ reaction. *The Journal of Chemical Physics* **2020**, *153*.
- [32] Duignan, T. T.; Parsons, D. F.; Ninham, B. W. Hydronium and hydroxide at the air–water interface with a continuum solvent model. *Chemical Physics Letters* **2015**, *635*, 1–12.
- [33] Skinner, L. B.; Huang, C.; Schlesinger, D.; Pettersson, L. G.; Nilsson, A.; Benmore, C. J. Benchmark oxygen–oxygen pair-distribution function of ambient water from x-ray diffraction measurements with a wide Q-range. *The Journal of chemical physics* **2013**, *138*.
- [34] Sujith, K.; Ramachandran, C. Carbon dioxide induced bubble formation in a CH 4–CO 2–H 2 O ternary system: a molecular dynamics simulation study. *Physical Chemistry Chemical Physics* **2016**, *18*, 3746–3754.
- [35] Piaggi, P. M.; Selloni, A.; Panagiotopoulos, A. Z.; Car, R.; Debenedetti, P. G. A first-principles machine-learning force field for heterogeneous ice nucleation on microcline feldspar. *Faraday Discussions* **2024**, *249*, 98–113.
- [36] Zhang, Z.; Li, H.; Shao, Y.; Gan, L.; Kang, F.; Duan, W.; Hansen, H. A.; Li, J. Molecular understanding of the critical role of alkali metal cations in initiating CO₂ electroreduction on Cu (100) surface. *Nature Communications* **2024**, *15*, 612.
- [37] Willow, S. Y.; Salim, M. A.; Kim, K. S.; Hirata, S. Ab initio molecular dynamics of liquid water using embedded-fragment second-order many-body perturbation theory towards its accurate property prediction. *Scientific reports* **2015**, *5*, 14358.
- [38] Prasetyo, N.; Hofer, T. S. Structure, dynamics, and hydration free energy of carbon dioxide in aqueous solution: a quantum mechanical/molecular mechanics molecular dynamics thermodynamic integration (QM/MM MD TI) simulation study. *Journal of Chemical Theory and Computation* **2018**, *14*, 6472–6483.
- [39] Martins-Costa, M. T.; Ruiz-López, M. F. Probing solvation electrostatics at the air–water interface. *Theoretical Chemistry Accounts* **2023**, *142*, 29.
- [40] Lam, R. K.; England, A. H.; Smith, J. W.; Rizzuto, A. M.; Shih, O.; Prendergast, D.; Saykally, R. J. The hydration structure of dissolved carbon dioxide from X-ray absorption spectroscopy. *Chemical Physics Letters* **2015**, *633*, 214–217.
- [41] Kumar, P. P.; Kalinichev, A. G.; Kirkpatrick, R. J. Hydrogen-bonding structure and dynamics of aqueous carbonate species from Car–Parrinello molecular dynamics simulations. *The Journal of Physical Chemistry B* **2009**, *113*, 794–802.
- [42] Kumar, N.; Servis, M. J.; Liu, Z.; Clark, A. E. Competitive interactions at electrolyte/octanol interfaces: A molecular perspective. *The Journal of Physical Chemistry C* **2020**, *124*, 10924–10934.
- [43] Jedlovszky, P.; Sega, M. Surface viscosity of liquid interfaces from Green–Kubo relations. *The Journal of Chemical Physics* **2024**, *160*.
- [44] Hantal, G.; Jedlovszky, P.; Sega, M. Local structure of liquid/vapour interfaces approaching the critical point. *Soft Matter* **2023**, *19*, 3773–3782.
- [45] SOKHAN, B. V.; Tildesley, D. The free surface of water: molecular orientation, surface potential and nonlinear susceptibility. *Molecular Physics* **1997**, *92*, 625–640.
- [46] Zhang, H.; Singer, S. J. Analysis of the subcritical carbon dioxide–water interface. *The Journal of Physical Chemistry A* **2011**, *115*, 6285–6296.
- [47] Chen, S.-H.; Singer, S. J. Molecular dynamics study of the electric double layer and nonlinear spectroscopy at the amorphous silica–water interface. *The Journal of Physical Chemistry B* **2019**, *123*, 6364–6384.
- [48] Verreault, D.; Allen, H. C. Bridging the gap between microscopic and macroscopic views of air/aqueous salt interfaces. *Chemical Physics Letters* **2013**, *586*, 1–9.
- [49] Hua, W.; Verreault, D.; Allen, H. C. Surface electric fields of aqueous solutions of NH₄NO₃, Mg (NO₃)₂, NaNO₃, and LiNO₃: implications for atmospheric aerosol chemistry. *The Journal of Physical Chemistry C* **2014**, *118*, 24941–24949.
- [50] da Rocha, S. R.; Johnston, K. P.; Westacott, R. E.; Rossky, P. J. Molecular structure of the water–supercritical CO₂ interface. *The Journal of Physical Chemistry B* **2001**, *105*, 12092–12104.
- [51] Servis, M. J.; Clark, A. E. Surfactant-enhanced heterogeneity of the aqueous interface drives water extraction into organic solvents. *Physical Chemistry Chemical Physics* **2019**, *21*, 2866–2874.
- [52] Kumar, N.; Clark, A. E. Unexpected inverse correlations and cooperativity in ion-pair phase transfer. *Chemical science* **2021**, *12*, 13930–13939.
- [53] Morita, A.; Koizumi, A.; Hirano, T. Recent progress in simulating microscopic ion transport mechanisms at liquid–liquid interfaces. *The Journal of Chemical Physics* **2021**, *154*.
- [54] Becker, M. R.; Loche, P.; Netz, R. R. Electrokinetic, electrochemical, and electrostatic surface potentials of the pristine water liquid–vapor interface. *The Journal of Chemical Physics* **2022**, *157*.
- [55] Yamada, H. Comparison of solvation effects on CO₂ capture with aqueous amine solutions and amine-functionalized ionic liquids. *The Journal of Physical Chemistry B* **2016**, *120*, 10563–10568.

